complex will have the higher redox potential.

Final Comments

Data have been reported in this study for 119 redox couples displayed in Figure 2. Allowing that agreement between calculated and observed values of <0.25 V represents good behavior, only nine redox couples are poorly fitted, possibly three for reasons of experimental error and six for more subtle reasons.[37] Certainly, most of the data reported here fit predicted potentials to within 0.15 V (Table II).

The appearance of a pair of lines for the $Re^{II/I}$ redox couple is unexpected; the observation suggests some important structural or electronic differences between the rhenium(I) species in the upper and lower lines. However, the possibility that the Re^{II}/Re^{I} line is really a curve cannot be excluded. It is therefore desirable to obtain data for $\sum E_L$ values in the intermediate range between the two lines. Such data should provide better statistics for the lower line or disprove the discontinuity. If two lines are present, then physical data are needed to define the differences between the complexes on each line.

Study of the electrochemistry of definitive seven-coordinate rhenium(III) species is clearly desirable. Some reversible electrochemistry has been observed with seven-coordinate hydride rhenium species.[13,38] Controlled-potential reduction studies of rhenium species of negative $\sum E_L$ values should prove especially interesting.

Acknowledgment. I am grateful for the continued financial support of the Natural Sciences and Engineering Research Council (Ottawa) and the Office of Naval Research (Washington). My appreciation is also extended to Drs. Armando Pombeiro and Mike Clarke for sharing prepublished information and for useful comments. I thank a reviewer for useful comments on the solvation energy problem.

(35) Due to uncertainty in the exact slope of the $Re^{III/II}$ correlation, this intercept value can only be considered approximate.
(36) Vanderheyden, J.-L.; Heeg, M. J.; Deutsch, E. *Inorg. Chem.* **1985**, *24*, 1666-73.
(37) The four poor $Re^{III/II}$ couples have already been discussed. The $Re^{II/I}$ couple for the species [Re(terpy)$(CO)_2$Cl] (terpy = 2,2′,2″-terpyridine)[45] is too high by 0.5 V and that for[51] *f*-Re$(CO)_3(NCMe)_3$, too low, by 0.5 V for no obvious reasons.
(38) Fanwick, P. E.; Leeaphon, M.; Walton, R. A. *Inorg. Chem.* **1990**, *29*, 676.
(39) Esjornson, D.; Bakir, M.; Fanwick, P. E.; Jones, K. S.; Walton, R. A. *Inorg. Chem.* **1990**, *29*, 2055.
(40) Bakir, M.; Fanwick, P. E.; Walton, R. A. *Polyhedron* **1987**, *6*, 907-13.
(41) Chatt, J.; Elson, C. M.; Hooper, N. E.; Leigh, G. J. *J. Chem. Soc., Dalton Trans.* **1975**, 2392.
(42) Fernanda, M.; Carvalho, N. N.; Pombeiro, A. J. L. *J. Chem. Soc., Dalton Trans.* **1989**, 1209-16.
(43) Morris, R. H.; Earl, K. A.; Luck, R. L.; Lazarowych, N. J.; Sella, A. *Inorg. Chem.* **1987**, *26*, 2674-83.
(44) Pombeiro, A. J. L. *Inorg. Chim. Acta* **1985**, *103*, 95-103.
(45) Juris, A.; Campagna, S.; Bidd, I.; Lehn, J.-M.; Ziessel, R. *Inorg. Chem.* **1988**, *27*, 4007-11.
(46) Treichel, P. M.; Williams, J. P. *J. Organomet. Chem.* **1977**, *135*, 39-51.
(47) Caspar, J. V.; Sullivan, B. P.; Meyer, T. J. *Inorg. Chem.* **1984**, *23*, 2104-9.
(48) Meyer, T. J. Personal communication, 1989.
(49) Leigh, G. J.; Morris, R. H.; Pickett, C. J.; Stanley, D. R.; Chatt, J. *J. Chem. Soc., Dalton Trans.* **1981**, 800.
(50) Luong, J. C.; Nadjo, L.; Wrighton, M. S. *J. Am. Chem. Soc.* **1978**, *100*, 5790.
(51) Brisdon, B. J.; Edwards, D. A.; Towell, I. M.; Moehring, G. A.; Walton, R. A. *J. Chem. Soc., Dalton Trans.* **1988**, 245.
(52) Bond, A. M.; Colton, R.; McDonald, M. E. *Inorg. Chem.* **1978**, *17*, 2842-7.
(53) Cameron, C. J.; Tetrick, S. M.; Walton, R. A. *Organometallics* **1984**, *3*, 240-7.
(54) Roncari, E.; Mazzi, U.; Seeber, R.; Zanello, P. *J. Electroanal. Chem. Interfacial Electrochem.* **1982**, *132*, 221-31.
(55) Heath, G. A.; Moock, K. A.; Sharp, D. W. A.; Yellowlees, L. J. *J. Chem. Soc., Chem. Commun.* **1985**, 1503-5.
(56) Trop, H. S.; Davison, A.; Carey, G. H.; DePamphilis, B. V.; Jones, A. G.; Davis, M. A. *J. Inorg. Nucl. Chem.* **1979**, *41*, 271-2.
(57) Gardiner, I. M.; Bruck, M. A.; Wexler, P. A.; Wigley, D. E. *Inorg. Chem.* **1989**, *28*, 3688-95.

Contribution from the School of Chemical Sciences and Department of Physics and Materials Research Laboratory, University of Illinois, Urbana, Illinois 61801, and Department of Chemistry, 0506, University of California at San Diego, La Jolla, California 92093-0506

Valence Trapping of Mixed-Valence $[Fe_3O(O_2CCH_3)_6(py)_3]\cdot S$ (S = Solvent) Complexes at High Pressure

James K. McCusker,[1,2] Ho G. Jang,[1] Maruta Zvagulis,[1] Walter Ley,[1] Harry G. Drickamer,*[1,3] and David N. Hendrickson*[,2]

Received August 22, 1989

The transformation from valence detrapped to valence trapped for two oxo-centered trinuclear iron acetate complexes is studied at pressures up to 95 kbar with the use of a diamond anvil cell. Variable-pressure ^{57}Fe Mössbauer spectra are presented for ^{57}Fe-enriched $[Fe_3O(O_2CCH_3)_6(py)_3]\cdot py$ (**1**) and $[Fe_3O(O_2CCH_3)_6(py)_3]\cdot CHCl_3$ (**2**), where py is pyridine. At 298 K and applied pressures less than ~20 kbar, each of the complexes gives a spectrum with a single quadrupole-split doublet, which indicates that complexes **1** and **2** are interconverting faster than the Mössbauer time scale under these conditions. Application of pressure in excess of ~80 kbar leads to both complexes becoming valence trapped, as indicated by two doublets in the Mössbauer spectrum with an area ratio of ~2:1 (Fe^{III}:Fe^{II}). At intermediate pressures, each of these complexes gives a Mössbauer spectrum that can be fit as a superposition of a valence detrapped doublet and a valence trapped four-line pattern. The nature of the pressure-induced transformations observed in complexes **1** and **2** is discussed with reference to the phase diagram derived from a spin-Hamiltonian theoretical approach that parametrizes intermolecular interactions in terms of the molecular field approximation.

Introduction

The study of intramolecular electron-transfer events in mixed-valence[4] complexes in the solid state has yielded exquisite details about the factors controlling electron-transfer processes.[5] The influence of nearby solvate molecules on the rate of electron

(1) School of Chemical Sciences, University of Illinois.
(2) University of California at San Diego.
(3) Department of Physics and Materials Research Laboratory, University of Illinois.
(4) Recent reviews: (a) Day, P. *Int. Rev. Phys. Chem.* **1981**, *1*, 149. (b) *Mixed-Valence Compounds, Theory and Applications in Chemistry, Physics, Geology and Biology*; Brown, D. B., Ed.; Reidel: Boston, MA, 1980. (c) Creutz, C. *Prog. Inorg. Chem.* **1983**, *30*, 1-73. (d) Richardson, D. E.; Taube, H. *Coord. Chem. Rev.* **1984**, *60*, 107.

0020-1669/91/1330-1985$02.50/0

transfer between donor and acceptor sites has been probed by studying triangular mixed-valence complexes of the composition $[Fe_3O(O_2CCH_3)_6(L)_3]\cdot S$, where L is a ligand such as pyridine (py) and S is a solvate molecule. The solvate molecule may affect the rate of intramolecular electron transfer in basically two different ways. Intermolecular interactions between Fe_3O complexes in the solid state have been shown to be important in determining whether a complex remains valence trapped or becomes valence detrapped as the temperature is increased. The size and shape of the solvate molecule affect intermolecular interactions between Fe_3O complexes.

The second and more interesting manner in which the solvate molecule S can influence the rate of intramolecular electron transfer in these Fe_3O complexes is more subtle than the first. Several $[Fe_3O(O_2CCH_3)_6(py)_3]\cdot S$ complexes have been found to crystallize in the *R*32 space group at room temperature. There are stacks of Fe_3O complexes with one solvate molecule sandwiched between pairs of Fe_3O complexes. Each Fe_3O complex has a small part of a solvation sphere in the crystalline environment. If the S···Fe_3O van der Waals interactions lead to an environment about the Fe_3O complex that is of lower symmetry than C_3, this will introduce energy differences between the vibronic states of the Fe_3O complex. Such an asymmetry will reduce the rate at which the Fe_3O complex can tunnel (i.e., electron transfer) between its vibronic states.

The only intensive property that has been varied to probe the dynamics and electronic structure of mixed-valence Fe_3O complexes is temperature. For several of these complexes, it has been found that the conversion from valence trapped to valence detrapped occurs in a phase transition.[5c,d,f,j,k] The complex $[Fe_3O(O_2CCH_3)_6(py)_3]\cdot py$ for example is valence trapped as a $Fe^{II}Fe^{III}_2$ complex below $\sim$100 K.[5g] As the temperature of this compound is increased, there is an abrupt appearance of some valence detrapped complexes at $\sim$112 K, as documented by Mössbauer spectroscopy.

Increasing the temperature above $\sim$112 K leads to an increase in the amount of detrapped species, and eventually by $\sim$190 K all complexes are interconverting faster than the Mössbauer time scale. This is particularly interesting, for heat capacity data show there is a first-order phase transition at $\sim$112 K, followed by a higher order phase transition that starts at $\sim$113 K and culminates at $\sim$190 K.[5d] The $\sim$113 to $\sim$190 K higher order phase transition also involves a cooperative onset of motion of the pyridine solvate molecules, as indicated by solid-state ^2H NMR spectra for crystals of $[Fe_3O(O_2CCH_3)_6(C_5D_5N)_3]\cdot C_5D_5N$. The onset of dynamics of the chloroform solvate structure in *R*32 symmetry $[Fe_3O(O_2CCH_3)_6(py)_3]\cdot CHCl_3$ has also very recently been shown[5k] to be coupled to valence detrapping of the Fe_3O complex. In this case, the two processes occur cooperatively in a single first-order phase transition.

The *R*32 symmetry Fe_3O complexes can be driven between three different phases by variations in temperature. Theoretical work[5f,6] suggests that there are interpenetrating sublattices, where every other complex is in either sublattice A or sublattice B. Accordingly, upon an increase in the temperature, $[Fe_3O(O_2CCH_3)_6(py)_3]\cdot py$ could be converting from ferrodistortive phase I to antiferrodistortive phase II in a first-order phase transition at $\sim$112 K.[6] The conversion from phase II to paradistortive phase III, which is expected to be of higher order, is suggested to occur in the $\sim$113 to $\sim$190 K range. As a result of different magnitudes of intermolecular interactions, $[Fe_3O(O_2CCH_3)_6(py)_3]\cdot CHCl_3$ may be directly converting in a first-order phase transition from ferrodistortive phase I to paradistortive phase III. It is interesting that the pyridine solvate $[Mn_3O(O_2CCH_3)_6(py)_3]\cdot py$ has very recently also been found[7] to exhibit only a single first-order phase transition, where there is appreciable long-range order in this valence detrapping phase transition.

There are two intensive properties, pressure and temperature, that play an important role in thermodynamics, since they largely affect, and often completely determine, the state of a system. All of the above thermally driven valence detrapping transformations were carried out at 1 atm of pressure. It was of interest to examine the effect of high pressure on $[Fe_3O(O_2CCH_3)_6(py)_3]\cdot py$ (**1**) and $[Fe_3O(O_2CCH_3)_6(py)_3]\cdot CHCl_3$ (**2**).

Experimental Section

Compound Preparation. ^{57}Fe-enriched (>98%) iron metal was purchased from MSD Chemical Co. Pyridine was dried by refluxing over BaO and fractionally distilled under an argon atmosphere. Chloroform (99+%) was used without further purification. All solvents and compounds were stored and manipulated under an argon atmosphere.

^{57}Fe-enriched $FeCl_2\cdot 4H_2O$ was prepared in the reaction of 30 mg of ^{57}Fe-enriched iron metal with the mixed solution of 1 mL of concentrated HCl and 3 mL of H_2O, which was carried out at 70–80 °C for 30 min. Evaporation and drying in vacuo gave 0.102 g of $FeCl_2\cdot 4H_2O$ (96% yield). A sample of ^{57}Fe-enriched $[Fe_3O(O_2CCH_3)_6(py)_3]\cdot py$ was prepared by dissolving 0.10 g of $FeCl_2\cdot 4H_2O$, 0.10 g of sodium acetate, and 0.3 mL of glacial acetic acid in 1.5 mL of H_2O. The reaction mixture was heated under reflux for 20 min with a constant stream of air bubbling through the solution. The dark brown product $[Fe_3O(O_2CCH_3)_6(H_2O)_3]$ (0.168 g) was obtained (58% yield) and then dissolved in $\sim$1 mL of pyridine, and the solution was stirred for 30 min at 50–60 °C in a glovebox under an argon atmosphere. After slow evaporation for 2 days, the solution was filtered and the precipitate dried briefly under vacuum. About 0.170 g of black crystalline $[Fe_3O(O_2CCH_3)_6(py)_3]\cdot py$ was obtained (68% yield).

A sample of ^{57}Fe-enriched $[Fe_3O(O_2CCH_3)_6(py)_3]\cdot CHCl_3$ was obtained by evaporating 2 mL of $CHCl_3$ containing 0.10 g of ^{57}Fe-enriched $[Fe_3O(O_2CCH_3)_6(py)_3]\cdot CHCl_3$.

^{57}Fe Mössbauer Spectroscopy. The high-pressure apparatus used in this study has been described previously.[8] The maximum amount of each ^{57}Fe-enriched sample was loaded into the diamond anvil cell to provide the maximum signal for collection of data. A small amount of mineral oil was then placed in the cell prior to closure to ensure quasihydrostatic conditions. Cell loading was done quickly in air, and in no case was there evidence of sample degradation due to oxidation. A typical run, involving collection of data at eight pressures, lasted approximately 3–4 weeks. At no time during any run was there evidence of cell leakage or loss of pressure.

Mössbauer spectra were collected in the constant-acceleration mode, by using a Ranger Scientific MS-900 Mössbauer spectrometer interfaced to an Apple IIe personal computer. The source used was a 20-mCi ^{57}Co point-source adsorbed into a Rh matrix (Amersham Corp.). The source was specially prepared on a pointed substrate so that the source could be moved as close as possible to the sample in the diamond anvil cell. All Mössbauer parameters are referenced to iron foil at 300 K. Data were fitted with Lorentzian peaks by using a modified version of a previously published program.[9]

Results and Discussion

Effects of Pressure. ^{57}Fe Mössbauer spectroscopy is well suited to monitor changes in electronic structure of a mixed-valence iron compound. Less than 1 mg of ^{57}Fe-enriched $[Fe_3O(O_2CCH_3)_6(py)_3]\cdot py$ (**1**) was loaded with a small amount of mineral oil into

(5) (a) Oh, S. M.; Hendrickson, D. N.; Hassett, K. L.; Davis, R. E. *J. Am. Chem. Soc.* **1984**, *106*, 7984. (b) Oh, S. M.; Hendrickson, D. N.; Hassett, K. L.; Davis, R. E. *J. Am. Chem. Soc.* **1985**, *107*, 8009. (c) Oh, S. M.; Kambara, T.; Hendrickson, D. N.; Sorai, M.; Kaji, K.; Woehler, S. E.; Wittebort, R. *J. Am. Chem. Soc.* **1985**, *107*, 5540. (d) Sorai, M.; Kaji, K.; Hendrickson, D. N.; Oh, S. M. *J. Am. Chem. Soc.* **1986**, *108*, 702. (e) Woehler, S. E.; Wittebort, R. J.; Oh, S. M.; Hendrickson, D. N.; Inniss, D.; Strouse, C. E. *J. Am. Chem. Soc.* **1986**, *108*, 2938. (f) Kambara, T.; Hendrickson, D. N.; Sorai, M.; Oh, S. M. *J. Chem. Phys.* **1986**, *85*, 2895. (g) Woehler, S. E.; Wittebort, R. J.; Oh, S. M.; Kambara, T.; Hendrickson, D. N.; Inniss, D.; Strouse, C. E. *J. Am. Chem. Soc.* **1987**, *109*, 1063. (h) Oh, S. M.; Wilson, S. R.; Hendrickson, D. N.; Woehler, S. E.; Wittebort, R. J.; Inniss, D.; Strouse, C. E. *J. Am. Chem. Soc.* **1987**, *109*, 1073. (i) Hendrickson, D. N.; Oh, S. M.; Dong, T.-Y.; Kambara, T.; Cohn, M. J.; Moore, M. F. *Comments Inorg. Chem.* **1985**, *4*, 329. (j) Sorai, M.; Shiomi, Y.; Hendrickson, D. N.; Oh, S. M.; Kambara, T. *Inorg. Chem.* **1987**, *26*, 223. (k) Jang, H. G.; Geib, S. J.; Kaneko, Y.; Nakano, M.; Sorai, M.; Rheingold, A. L.; Montez, B.; Hendrickson, D. N. *J. Am. Chem. Soc.* **1989**, *111*, 173.

(6) Stratt, R. M.; Adachi, S. H. *J. Chem. Phys.* **1987**, *86*, 7156.

(7) (a) Jang, H. G.; Vincent, J. B.; Nakano, M.; Huffman, J. C.; Christou, G.; Sorai, M.; Wittebort, R. J.; Hendrickson, D. N. *J. Am. Chem. Soc.* **1989**, *111*, 7778. (b) Nakano, M.; Sorai, M.; Vincent, J. B.; Christou, G.; Jang, H. G.; Henrickson, D. N. *Inorg. Chem.* **1989**, *28*, 4608.

(8) Jurgensen, C. W.; Drickamer, H. G. *Phys. Rev. B* **1984**, *30*, 7202.

(9) Chrisman, B. L.; Tumolillo, T. A. *Comput. Phys. Commun.* **1971**, *2*, 322.

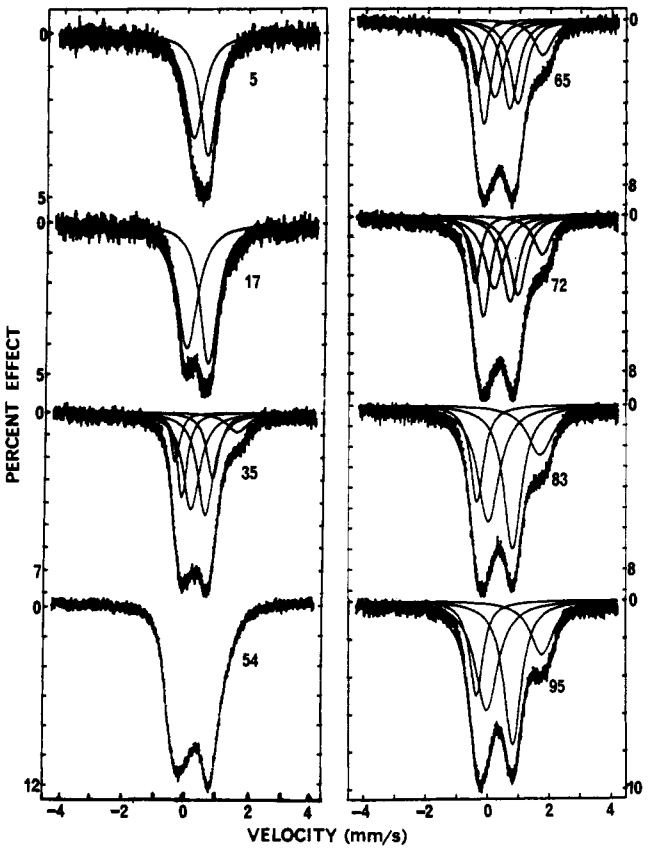

Figure 1. Variable-pressure ^{57}Fe Mössbauer spectra of an ^{57}Fe-enriched sample of $[Fe_3O(O_2CCH_3)_6(py)_3]\cdot py$ (**1**). The numbers marked on the spectra correspond to the applied pressure in units of kbar.

a diamond anvil cell. Room-temperature Mössbauer spectra were run at different applied pressures in the range 5–95 kbar; see Figure 1 (1 kbar = 986.92 atm = 0.1 GPa). It is evident that this compound is converting from being valence detrapped at 5 kbar to valence trapped at 95 kbar. Also, upon release of the pressure in the diamond anvil cell, the Mössbauer spectrum returns to the detrapped pattern found at 5 kbar, but with significant broadening of the spectrum (vide infra). A run on a second sample of complex **1** showed that the spectral changes observed are reproducible. In a qualitative sense, the changes in the spectrum seen upon increasing the pressure from 5 to 95 kbar are similar to those occurring upon decreasing the sample temperature from 320 to 11 K with the sample maintained at 1 atm. That is, the spectra change from a detrapped doublet at low pressure (high temperature) to a valence trapped pattern at high pressure (low temperature). There are some appreciable differences such as the much greater line widths observed upon application of pressure. These greater line widths likely reflect distributions in defect structure (e.g. dislocations) created by the application of pressure.

Basically there are two different ways to analyze the pressure dependencies seen in the Mössbauer spectrum for complex **1**. The spectra at intermediate pressures could be either least-squares fit to Lorentzian line shapes or simulated by a relaxation model. After carefully weighing all of the factors, we decided to take the former approach for the following reasons. First, it is important to note that, for all of the $[Fe_2^{III}Fe^{II}O(O_2CCH_3)_6(L)_3]\cdot S$ complexes studied, three different packing arrangements have been noted. For the L = pyridine or 4-methylpyridine complexes there are stacks of Fe_3O complexes with $R32$ symmetry above a certain temperature.[5e,g,k] For L = 3-methylpyridine (3-Me-py) the Fe_3O complexes are arranged two-dimensionally in layers with the solvate molecules (3-Me-py, toluene, or benzene) located in an open space made by three neighboring Fe_3O complexes.[5h] The Fe_3O complexes in $[Fe_3O(O_2CCH_3)_6(4\text{-Et-py})_3]\cdot 4\text{-Et-py}$ ($C2/c$ space group) are not arranged in either stacks or layers.[5b] Both the stacked ($R32$ space group) and the layered complexes have been shown with heat capacity results to exhibit phase transitions.[5c,d,f,j,k] The temperature dependencies seen for the Mössbauer spectra of the stacked and layered Fe_3O complexes are similar. At low temperatures two doublets in a 2:1 ratio (Fe^{III}:Fe^{II}) are found for each complex. As the temperature is increased, a third doublet with parameters characteristic of a valence detrapped species appears *very abruptly*. A detailed analysis of the spectra for $[Fe_3O(O_2CCH_3)_6(py)_3]\cdot py$ has been presented[5e] to show that the temperature dependence of the Mössbauer spectrum is not consistent with a simple relaxation model. First, it was shown that in the 61–114 K region the spectra could be fit with three doublets (Fe^{III}, Fe^{II}, and valence detrapped) with quite reasonable line widths. Second, simulations of the Mössbauer spectra were carried out by employing a three-site relaxation model. These simulated spectra did *not* mimic well the temperature dependence seen.[5e] Third, from variable-temperature ^2H NMR data on an oriented single crystal of $[Fe_3O(O_2CCD_3)_6(py)_3]\cdot py$, it was definitively concluded that the rate of the process that averages the Fe^{III} and Fe^{II} valences in this complex is less than 3.1×10^4 s^{-1} at ~173 K.[5g] Since the ^{57}Fe Mössbauer spectra for this complex show the rate of this valence detrapping process is greater than $\sim 10^8$ s^{-1} at ~190 K (one doublet), a change from less than 3.1×10^4 s^{-1} to greater than $\sim 10^8$ s^{-1} in a ~17-deg interval is not at all consistent with a simple relaxation model. In such a model it is tacitly assumed that for an individual molecule there is a potential energy diagram with barriers between different states. With an increase in temperature, the molecule is able to overcome the barriers and the rate of the interconversion process increases. However, it is clear that in the stacked and layered complexes valence detrapping occurs cooperatively in phase transitions. There is a catastrophic event, and the kinetics are those of domain walls moving in the crystal, not individual molecules overcoming barriers. A dramatic example of just how abruptly valence detrapping can occur is found with $[Mn_3O(O_2CCH_3)_6(py)_3]\cdot py$.[7] A plot of the excess entropy gain versus temperature shows that ~67% of the total entropy gain occurs in a ~5-deg interval in a first-order phase transition that involves valence detrapping in the Mn_3O complex and the onset of motion of the pyridine solvate molecule.

Further evidence that "lattice dynamics" are determining the temperature dependence of the Mössbauer spectra of mixed-valence complexes is available. It has been shown[5b] that for $[Fe_3O(O_2CCH_3)_6(4\text{-Et-py})_3]\cdot 4\text{-Et-py}$ there is no evidence of relaxation effects in the Mössbauer spectra. Only two doublets are seen in each Mössbauer spectrum in the 6.5–298 K range. There is a valence-averaging process present. However, the Fe^{II} and Fe^{III} doublets just move together to become one average-valence doublet *without any evidence of line broadening*. These spectra do *not* need to be simulated by a relaxation model. If the rate of the valence detrapping process is increasing with increasing temperature and goes through the range ($\sim 10^6$–10^9 s^{-1}) that should affect the line shapes of Mössbauer signals, line broadening and coalescence should be seen. It is not seen. The inescapable conclusion is that, whatever the process affecting the Mössbauer spectrum for the above complex, it is at all temperatures faster than the ^{57}Fe Mössbauer technique can sense. It must be emphasized that several mixed-valence biferrocenium salts have been reported[10] to show this same type of temperature dependence of Mössbauer spectra. It was for the above reasons that we decided not to simulate the spectra of Figure 1 with a relaxation model, but to fit the spectra with Lorentzian line shapes. Even if a relaxation model were relevant to the pressure dependence observed for the Mössbauer spectrum, the very broad features observed in the 35–83 kbar region would make such a relaxation simulation not very definitive. It is very likely that the application of pressure leads to an appreciable increase in defects (dislocations) in the crystallites. This would lead to appreciable distributions in environments about the Fe_3O complexes and broad Mössbauer lines.

It became apparent during least-squares fitting of the 35–95 kbar Mössbauer spectra of complex **1** to Lorentzian line shapes

(10) Webb, R. J.; Geib, S. J.; Staley, D. L.; Rheingold, A. L.; Hendrickson, D. N. *J. Am. Chem. Soc.* **1990**, *112*, 5031 and references therein.

Table I. Mössbauer Fitting Parameters for $[Fe_3O(O_2CCH_3)_6(py)_3]\cdot py$

P, kbar		IS, mm/s	QS, mm/s	area, %
5	Fe^{av}	0.577 (3)	0.451 (7)	100
17	Fe^{av}	0.515 (3)	0.695 (5)	100
35	Fe^{III}	0.549 (9)	0.99 (2)	28.8 (3)
	Fe^{II}	0.83 (2)	2.00 (3)	14.4 (1)
	Fe^{av}	0.58 (2)	0.46 (4)	56.6 (5)
54[a]				
65	Fe^{III}	0.54 (1)	1.09 (3)	40.2 (2)
	Fe^{II}	0.816 (8)	2.15 (2)	19.6 (1)
	Fe^{av}	0.58 (2)	0.48 (5)	40.2 (2)
72	Fe^{III}	0.54 (2)	1.12 (3)	39.6 (3)
	Fe^{II}	0.807 (7)	2.18 (2)	20.2 (1)
	Fe^{av}	0.59 (3)	0.51 (6)	40.2 (3)
83	Fe^{III}	0.545 (3)	0.791 (5)	66.8 (4)
	Fe^{II}	0.802 (6)	2.05 (1)	33.4 (2)
95	Fe^{III}	0.519 (3)	0.843 (6)	66.8 (4)
	Fe^{II}	0.831 (5)	2.132 (9)	33.4 (2)

[a] The features in this spectrum are just too broad and overlapping to permit a good least-squares fit.

that there are two ways in which to fit these spectra. These two different schemes for fitting the Mössbauer spectra are referred to as scheme 1 and scheme 2. The data discussed in this paper for both complexes **1** and **2** are those derived from scheme 2. The fundamental difference between the scheme 1 and scheme 2 fittings is in the positioning of the negative-velocity component of the Fe^{II} doublet relative to the negative-velocity component of the Fe^{III} doublet. In scheme 1 the Fe^{II} signal is located at higher energy; in scheme 2 the locations are reversed, with the Fe^{II} signal occurring at the most negative velocity (lowest energy) position. Although this seems like a fairly minor distinction, the resulting trends in isomer shift and ΔE_Q with increasing pressure, as well as the overall qualities of the fits, are affected. The most dramatic difference in the observed trends was seen for the Fe^{II} isomer shift. With scheme 2, the Fe^{II} isomer shift remains relatively unchanged with pressure: 0.83 (2) mm/s at 35 kbar to 0.831 (5) mm/s at 95 kbar. Although the isomer shift will generally exhibit a decrease with increasing pressure,[11] slight increases have been noted in compounds that exhibit a fair degree of π-bonding.[11a,h,i] Thus, the trends observed for fitting scheme 2 are in accord with what has been reported previously. However, the fitting parameters derived from fitting scheme 1 for complex **1** indicate a very pronounced increase in the Fe^{II} isomer shift with increasing pressure: 1.1 (1) mm/s versus iron foil at 35 kbar and 1.9 (1) mm/s at 95 kbar. Such a large increase in isomer shift with increasing pressure does not have any precedent in the literature, leading us to conclude that only fitting scheme 2 gives physically reasonable parameters.

Fitting parameters are given in Table I for the Mössbauer spectra of complex **1** in the 5–95-kbar range. It is clear that at 5 and 17 kbar only a valence detrapped doublet is present. Also, the 83- and 95-kbar spectra are readily fit with a "valence trapped pattern" with two doublets in an area ratio of 2:1 (Fe^{III}:Fe^{II}). The spectra obtained in the intermediate range of 35–72 kbar presented more of a challenge. Least-squares fits of these four spectra to only two quadrupole-split doublets are not at all satisfactory when the area ratio of the two doublets is constrained to 2:1. Physically unrealistic area ratios result when the areas of the two doublets are allowed to be independent; for example, fitting the 35-kbar spectrum to two unrestricted doublets gives an area ratio of 3.6:1.0. In short, the only physically realistic way to fit these spectra is to least-squares fit each spectrum to three doublets in fitting scheme 2, that is, a superposition of a valence trapped 2:1 two-doublet pattern and a single-doublet pattern for valence detrapped species. The resulting parameters are given in Table I. It is curious to note that although the values obtained for $\delta(Fe^{av})$ are intermediate between those for Fe^{II} and Fe^{III}, the values for ΔE_Q for Fe^{av} appear anomalously small. However, if one examines the asymmetry of the Fe^{II} and Fe^{III} signals at high pressure, it is clear that the signs of the EFG tensors for these two sites are opposite. The time-averaged Fe^{av} signal then, representing an average EFG tensor, will yield values for ΔE_Q that are collapsed

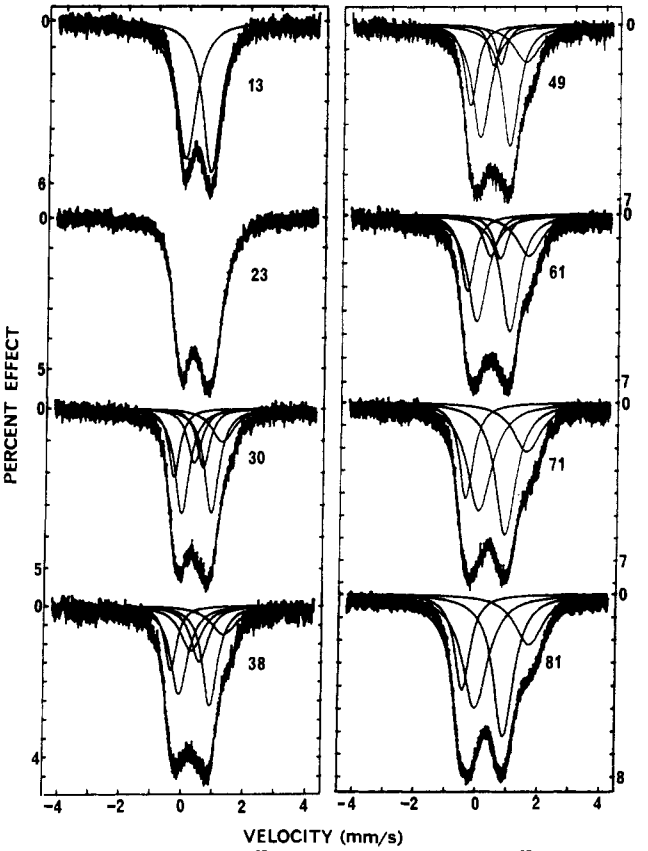

Figure 2. Variable-pressure ^{57}Fe Mössbauer spectra of an ^{57}Fe-enriched sample of $[Fe_3O(O_2CCH_3)_6(py)_3]\cdot CHCl_3$ (**2**). The numbers marked on the spectra correspond to the applied pressure in units of kbar.

Table II. Mössbauer Fitting Parameters for $[Fe_3O(O_2CCH_3)_6(py)_3]\cdot CHCl_3$

P, kbar		IS, mm/s	QS, mm/s	area, %
13	Fe^{av}	0.457 (2)	0.811 (4)	100
23[a]				
30	Fe^{III}	0.51 (2)	0.96 (3)	49.8 (5)
	Fe^{II}	0.55 (5)	1.6 (1)	25.0 (2)
	Fe^{av}	0.57 (2)	0.28 (5)	25.2 (2)
38	Fe^{III}	0.52 (3)	1.00 (6)	46.6 (9)
	Fe^{II}	0.60 (7)	1.7 (1)	23.3 (5)
	Fe^{av}	0.54 (7)	0.3 (1)	30.2 (7)
49	Fe^{III}	0.54 (1)	0.96 (3)	58.4 (6)
	Fe^{II}	0.63 (3)	1.82 (6)	29.2 (3)
	Fe^{av}	0.58 (1)	0.24 (3)	12.4 (1)
61	Fe^{III}	0.52 (2)	1.08 (4)	55.8 (5)
	Fe^{II}	0.67 (2)	2.01 (5)	27.8 (2)
	Fe^{av}	0.57 (3)	0.32 (5)	16.4 (1)
71	Fe^{III}	0.545 (4)	0.860 (7)	66.8 (6)
	Fe^{II}	0.672 (8)	1.99 (2)	33.4 (3)
81	Fe^{III}	0.528 (3)	0.927 (6)	66.8 (4)
	Fe^{II}	0.728 (7)	2.16 (1)	33.4 (2)

[a] The features in this spectrum are just too broad and overlapping to permit a good least-squares fit.

(11) (a) Drickamer, H. G.; Vaughan, R. W.; Champion, A. R. *Acc. Chem. Res.* **1969**, *2*, 40. (b) Champion, A. R.; Vaughan, R. W.; Drickamer, H. G. *J. Chem. Phys.* **1967**, *47*, 2583. (c) Fischer, D. C.; Drickamer, H. G. *J. Chem. Phys.* **1971**, *54*, 4825. (d) Bargeron, C. B.; Drickamer, H. G. *J. Chem. Phys.* **1971**, *55*, 3471. (e) Long, G. J.; Becker, L. W.; Hutchinson, B. B. *Adv. Chem. Ser.* **1982**, *194*, 453. (f) Long, G. J.; Hutchinson, B. B. *Inorg. Chem.* **1987**, *26*, 608. (g) McCusker, J. K.; Zvagulis, M.; Drickamer, H. G.; Hendrickson, D. N. *Inorg. Chem.* **1989**, *28*, 1380. (h) Drickamer, H. G.; Bastron, V. C.; Fiscker, D. C.; Grenoble, D. C. *J. Solid State Chem.* **1970**, *2*, 94. (i) Grenoble, D. C.; Frank, C. W.; Bargeron, C. B.; Drickamer, H. G. *J. Chem. Phys.* **1971**, *55*, 1633.

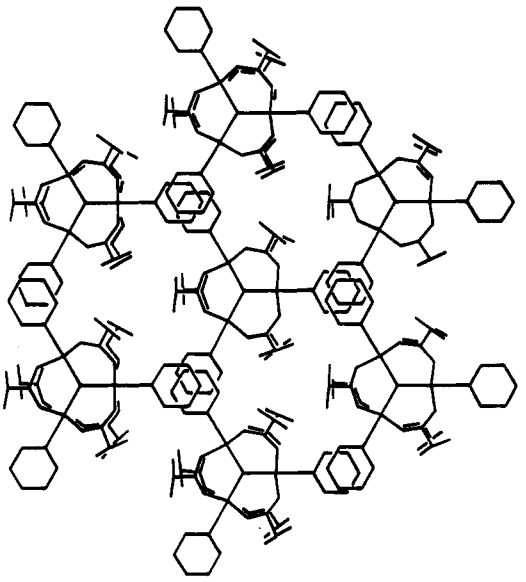

Figure 3. Schematic view down the stacking axis (*c* axis) of the packing arrangement for the *R*32 symmetry Fe_3O–acetate complexes.

relative to the Fe^{II} and Fe^{III} signals. This accounts for the small value found for ΔE_Q^{av}. It is important to note that the spectra obtained for the 1-atm sample in the 117–168 K region were fit in this same manner,[5g] as were variable-temperature spectra for several other Fe_3O complexes.[5j]

Variable-pressure Mössbauer spectra run for $[Fe_3O(O_2CCH_3)_6(py)_3]\cdot CHCl_3$ (**2**) are shown in Figure 2. The pressure dependence is similar to that seen for complex **1**. In the case of complex **2** only the lowest pressure spectrum taken at 13 kbar could be fit well by a single doublet. The important point to note regarding these spectra is that complex **2** shows at a lower pressure than does complex **1** the appearance of the "superposition spectrum" (see Table II). Complex **2** also becomes valence trapped at a pressure lower than that needed to trap complex **1**. This ~10-kbar shift in transition pressures relative to complex **1** can be accounted for qualitatively in the context of a phase diagram based on variable-temperature studies of these systems.

Nature of Pressure-Induced Transformations. The intermolecular interactions that are responsible for the thermally induced phase transitions observed for complexes **1** and **2** have been discussed in theoretical papers.[5f,6] Although the specific effect of a solvate molecule was not considered in either model, the results can be used at least qualitatively in the present study. It is important first to appreciate the types of intermolecular interactions that are present in the *R*32 symmetry Fe_3O complexes. A schematic view of the packing arrangement present in these complexes is shown in Figure 3. There are stacks of Fe_3O complexes along the *c* axis. Each stack is surrounded by six other stacks of Fe_3O complexes. As is evident in Figure 3, the main intermolecular interaction between two Fe_3O complexes comes in the form of an overlapping of pyridine ligands, leading to stacks of pyridine ligands. This py···py overlapping occurs between two Fe_3O complexes in neighboring stacks. Intermolecular interactions between two Fe_3O complexes in the same stack are weaker and are propagated by the solvate molecule S, which is sandwiched between pairs of Fe_3O molecules in the same stack.

The py···py intermolecular interactions have been treated by the molecular field approximation. Stratt and Adachi[6] took the insightful approach of employing a spin-type Hamiltonian, which leads logically to the idea of two interpenetrating sublattices of Fe_3O complexes. Figure 4 shows the phase diagram that results for these complexes. The intermolecular interaction energies that serve as variable parameters for the phase diagram are J_0 (≡0), J_1, J_2, and J_3, which gauge, respectively, the energies of two neighboring molecules, both of which are undistorted, both of which are distorted parallel to each other, only one of which is distorted, and both of which are distorted but are at an angle of $2\pi/3$ with respect to each other. There are actually two independent Hamiltonian parameters, J_2/J_1 and J_3/J_1, but it was found that the latter has no qualitative effect beyond changing the shape of the I–IV phase boundary in Figure 4. The interaction energy J_1 can be qualitatively thought of as the tendency for distorted molecules to align with the sense of molecular distortion parallel (also referred to as strain-dipole effects). J_2 is best thought of as simply the interaction energy resulting from py···py overlap. Thus, it is the variation in these two parameters as pressure is increased that needs to be considered.

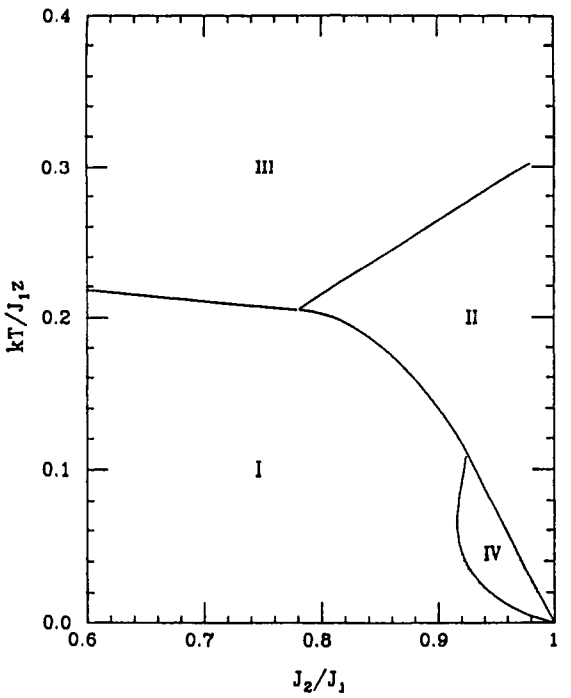

Figure 4. Phase diagram calculated by Stratt and Adachi[6] employing a mean-field theory to account for the phase transitions in mixed-valence Fe_3O complexes that crystallize in the *R*32 space group. The vertical axis is temperature plotted in units of k/J_1z, where k is the Boltzmann constant, z is the number of Fe_3O complexes surrounding each Fe_3O complex, and J_1 is the interaction energy of two neighboring complexes, both of which are distorted parallel to each other. The horizontal axis is the ratio of the "antiferromagnetic" (J_2) to the "ferromagnetic" (J_1) coupling, where J_2 is the interaction energy for two neighboring complexes, one distorted and the other undistorted.

In reference to the phase diagram in Figure 4, all Fe_3O complexes in phase I are valence trapped, and because of strain dipoles, the sense of distortion of each Fe_3O is the same. Phase I could be described as the ferrodistortive phase; in terms of a Mössbauer spectrum, one would anticipate a valence trapped, two-doublet pattern. In phase II (antiferrodistortive phase) two interpenetrating sublattices exist where one sublattice has valence trapped complexes and the sense of distortion (i.e., which ion is the Fe^{II} ion) is random. The other sublattice has an appreciable number of undistorted (delocalized) complexes mixed with randomly oriented trapped-valence complexes. This will translate into a six-line Mössbauer spectrum: two doublets in a 2:1 ratio corresponding to the valence trapped sublattice and one doublet for the delocalized species. In phase III (paradistortive phase) there is a random distribution of distorted and undistorted complexes, where each Fe_3O complex is probably tunneling rapidly between its three or four vibronic states. If the rate of electron transfer is faster than the ^{57}Fe Mössbauer time scale ($\sim 10^7$ s^{-1}), only one doublet will be observed. Phase IV was described as having two sublattices as in phase II, but with both sublattices "ferromagnetic" and distorted in the same direction. Only the I–III, I–II, and IV–II phase boundaries give first-order transitions. The other lines correspond to second-order transitions.

The pressure dependence of the Mössbauer spectra for complexes **1** and **2** can be interpreted qualitatively with Stratt and Adachi's phase diagram by analogy with what is known about their temperature dependence. At temperatures below ~100 K,

both complexes are in the trapped-valence ferrodistortive phase I. Heat capacity results[5d,g] for the pyridine solvate complex **1** show that it undergoes a first-order phase transition at ~112 K, presumably between phases I and II. These same data show there is a higher order phase transition starting at ~114 K and culminating at ~190 K. This could involve the transition from phase II to phase III. On the other hand, the heat capacity data for the chloroform solvate complex **2** only shows there is one phase transition present, which has two heat capacity peaks closely centered at 207.14 and 208.19 K.[5k] The appearance of the C_p versus temperature data for complex **2** does suggest the presence of appreciable first-order character in the ~208 K phase transition. It was concluded[5k] that if the phase diagram in Figure 4 is appropriate for these complexes, then complex **2** is directly converting from phase I to phase III in a first-order phase transition. This indicates that J_2/J_1 is smaller for complex **2** than for complex **1** and indicates relative "starting points" for both complexes in terms of the phase diagram in Figure 4.

With increasing pressure at 298 K, complexes **1** and **2** are converting from valence detrapped paradistortive phase III eventually to valence trapped phase I. It is difficult to decide whether one or both complexes go directly from phase III to phase I, or go through a phase II description, since the order of the transitions is unknown in the absence of variable-pressure heat capacity data. Because both complexes exhibit similar pressure-dependent Mössbauer spectra, where at intermediate pressure the spectra are superpositions of signals for trapped and detrapped species, it is tempting to say that both complexes **1** and **2** do experience the intermediacy of phase II. There are differences in pressure at which each complex enters a given phase. The pyridine solvate **1** converts from phase III to phase II at ~35 kbar and to phase I at ~83 kbar. The responses of the chloroform solvate are shifted 10 kbar to lower pressure; the III–II conversion occurs at ~23 kbar and the II–I conversion at ~71 kbar. This is likely a consequence of both the differences in the variation of J_2/J_1 with changing pressure as well as the nominal difference in the initial value of J_2/J_1 for the two complexes.

To understand the above observations in the context of Stratt and Adachi's model,[6] it is important to consider how the interaction parameters J_1 and J_2 might change with increasing pressure. Variable-temperature X-ray structural data indicate that decreasing the temperature of the $R32$ symmetry Fe_3O complexes results in a substantial decrease in the volume of the unit cell and that it is the c axis (stacking axis) which contracts the most. For example, X-ray structural data[5e] for the benzene solvate $[Fe_3O(O_2CCH_3)_6(4\text{-Me-py})_3]\cdot C_6H_6$ show that from 295 to 133 K the volume of the $R32$ crystal decreases by 5.65%. Most of this decrease occurs in the c axis, which decreases by 3.70%, whereas the a and b axes only decrease by 0.91%. It is therefore reasonable to assume that the application of hydrostatic (isotropic) pressure will probably result in compression predominantly along the c axis. This will result in substantially increased py···py intermolecular interactions, which corresponds to an increase in the value of J_2. As the lattice volume is decreased, J_1 will likely also increase somewhat, since increased intermolecular contacts will tend to favor alignment of strain dipoles. However, this change would not be expected to be as dramatic as the increased π–π overlap of the pyridine ligands. Thus, in general, the J_2/J_1 parameter would be expected to initially increase with increasing pressure.

The next step would be to modify the phase diagram in Figure 4 to account for the effects of applied pressure. Upon an increase in pressure, the phase boundary lines would be extended out from the present diagram. This would generate a three-dimensional grid in J_2/J_1, kT/J_1z, and some pressure functionality $f(P)$. If J_2/J_1 effectively increases with pressure, the triple point corresponding to the coexistence of phases I, II, and III would likely move to smaller values of J_2/J_1 in $f(P)$. As a result, *both* complexes **1** and **2** would upon application of pressure experience the intermediary phase II, consistent with the Mössbauer results. This is to be contrasted with the variable-temperature results, which suggest that complex **2** converts directly from phase I to phase III. A more instructive, though *strictly* qualitative, way to view this in the context of the current phase diagram is to liken an increase in pressure to a decrease in temperature, thereby allowing us to project onto Figure 4 a ∂P trajectory. It cannot be overemphasized that such an analogy is employed *only* to illustrate a possible contour in $f(P)$.

At 298 K, complex **1** crystallizes with $R32$ symmetry. The molecular stacking axis is the c axis with c = 11.074 (3) Å.[10] Complex **2** also crystallizes in $R32$, but at 298 K has a significantly shorter c axis, c = 10.488 (3) Å,[5k] implying a shorter py–py distance (cf. ref 8). Furthermore, the py···py intermolecular overlap in complex **2** is more eclipsed than that found for complex **1**. These factors will likely combine under the influence of pressure to result in a faster increase in $\partial(J_2/J_1)/\partial P$ for complex **2** relative to complex **1**. In terms of Figure 4, one can project a positively sloped line originating in phase III at low pressures and crossing into phase II at intermediate pressures. Depending on the relative slopes of $\partial(J_2/J_1)/\partial P$ for the two compounds, it is certainly possible that complex **2** would enter phase II at a lower pressure than complex **1**.

The transition of complex **2** from phase II to phase I can be accounted for in a qualitative sense if one examines the nature of the J_2 parameter more closely. Although J_2 will increase with increasing py–py overlap, at some point this interaction will become destabilizing due to π–π repulsion. Because of the eclipsed configuration of the pyridine ligands in complex **2**, this factor could become important at higher pressures. Thus, the same interaction that causes a rapid increase in J_2/J_1 at low and intermediate pressures could lead to a destabilization and subsequent decrease in J_2/J_1 at high pressure. The resulting bell-shaped contour in $f(P)$ would bring complex **2** from phase II into phase I. Again, the relative pressures for the II → I transformation in the two complexes will depend on the specific shapes of the $f(P)$ contours and are difficult to infer on the basis of the present data.

Acknowledgment. This work was supported in part by National Institutes of Health Grant HL13652 and in part by the Materials Science Division, Department of Energy, under Contract DE-AC02-76ER01198.